applied sciences

MDPI

Article

Effective Adsorption of Hexavalent Chromium and Divalent Nickel Ions from Water through Polyaniline, Iron Oxide, and Their Composites

Amir Muhammad [1], Anwar ul Haq Ali Shah [1] and Salma Bilal [2,3,*]

[1] Institute of Chemical Sciences, University of Peshawar, Peshawar 25120, Pakistan; amirics2015@gmail.com (A.M.); anwarulhaqalishah@uop.edu.pk (A.u.H.A.S.)
[2] National Centre of Excellence in Physical Chemistry, University of Peshawar, Peshawar 25120, Pakistan
[3] TU Braunschweig Institute of Energy and Process Systems Engineering, Franz-Liszt-Straße 35, 38106 Braunschweig, Germany
* Correspondence: s.bilal@tu-braunschweig.de; Tel.: +49-531-39163651

Received: 22 March 2020; Accepted: 6 April 2020; Published: 21 April 2020

Abstract: Water pollution caused by industrial wastes containing heavy metals and dyes is a major environmental problem. This study reports on the synthesis, characterization, and utilizations of Polyaniline (PANI) and its composites with Fe_3O_4 for the removal of hexavalent chromium Cr(VI) and divalent nickel Ni(II) ions from water. The adsorption data were fitted in Freudlich, Langmuir, Tempkin, Dubbanin–Ruddishkawich (D–R), and Elovich adsorption isotherms. The Freundlich isotherm fits more closely to the adsorption data with R^2 values of 0.9472, 0.9890, and 0.9684 for adsorption of Cr(VI) on Fe_3O_4, PANI, and PANI/Fe_3O_4 composites, respectively, while for adsorption of Ni(II) these values were 0.9366, 0.9232, and 0.9307 respectively. The effects of solution pH, initial concentration, contact time, ionic strength, and adsorbent dosage on adsorption behavior were investigated. The adsorption ability of composites was compared with pristine PANI and Fe_3O_4 particles. Activation energy and other thermodynamic properties such as changes in enthalpy, entropy, and Gibbs free energy indicated spontaneous and exothermic adsorption.

Keywords: hexavalent chromium; divalent nickel; kinetic study; adsorption isotherm; thermodynamic study

1. Introduction

Rapid increases in industrialization for the production of various products such as medicine, cloth, leather, paints, cement, and fertilizers are necessary to fulfill the basic needs of people in the modern world [1–4]. The effluents coming from these industries include several types of dyes and heavy metals. Mostly these effluents are added into nearby streams, canals, and rivers without any treatment. One of the very toxic elements in these effluents is chromium. It exists in various oxidation states such as Cr(II), Cr(III), Cr(IV), Cr(V), and Cr(VI) but trivalent Cr(III) and hexavalent Cr(VI) are environmentally stable [5].

Hexavalent chromium (Cr(VI)) is about 500 to 1000 times more toxic than its trivalent form, i.e., Cr(III), because of its high solubility and high mobility in almost the whole pH range of its solution [6]. Among toxic pollutants, Cr(VI) has been listed as a priority by the U.S. Environmental Protection Agency (EPA) [7]. It exists as oxyanions (CrO_4^{2-}, $Cr_2O_7^{2-}$, $HCrO_4^-$) in aqueous environments, and diffuses through cell membranes into living tissues and oxidize biological molecules. Accumulation of Cr(VI) in living tissues even in a very small concentration may cause severe neurological or physiological damage. The maximum permissible concentration of Cr(VI) in water is about 0.05 $mg{\cdot}L^{-1}$ as accepted by the World Health Organization (WHO) [8]. Perforation of the eardrums and the nasal septum, skin

lesions, ulceration, lung cancer, and a decrease in spermatogenesis are the most common effects caused by hexavalent chromium [9].

Nickel is also considered a significant heavy metal and is the fifth most abundant element in the Earth's crust after oxygen, magnesium, silicon, and iron. It is used in various industries such as stainless steel, automotive, hydrogenated oils, fertilizers like super phosphates, and food products [10]. Although it resists air, water, and alkali corrosion, it dissolves easily in dilute mineral acids. It can exist in several oxidation states such as -1, +1, +2, +3, and +4 but the most prominent oxidation state of nickel is +2. Although nickel is not toxic in low concentrations, it becomes harmful to both animals and human beings at high concentrations [11]. The World Health Organization (WHO) has recommended the maximum permissible value of nickel in drinking water as 0.02 $mg{\cdot}L^{-1}$ [12]. Among various adverse effects of nickel-containing compounds are allergies like contact dermatitis, cardiovascular diseases, respiratory tract cancer, kidney diseases, and lung fibrosis [13].

The presence of both hexavalent chromium Cr(VI) and divalent nickel Ni(II) in water even in very low concentrations contaminates it and makes it unsafe for drinking. Therefore, removal of these heavy metals is very important to make water safe. Several techniques such as flocculation, precipitation, ozonation, chemical coagulation, reverse osmosis, electro dialysis, and adsorption are used to remove heavy metals from aqueous environments [14–19]. However, among these techniques, adsorption is the most effective because of economic feasibility, its high efficiency, and simplicity of design. Moreover, adsorbents used for the removal of pollutants can be regenerated through desorption [20].

A number of adsorbents such activated carbon, rice husk, clay, sand, and saw dust can be used to remove these heavy metals from aqueous environments [21–23]. In the last few years, some conducting polymers like polythiophene (PT), polypyrrol (PPY), polyacrylonitril (PAN), and polyaniline (PANI) have been used as adsorbents for removal of heavy metals and dyes from aqueous solutions [24–26]. Among conducting polymers, PANI has been used much more frequently because of its easy synthesis from low cost material and has proven to be much friendlier to environment.

Various methods such as interfacial, self-assembly, seedling, oxidation through enzymes, and chemical and electro-chemical oxidation have been used to synthesize PANI [27–31]. However, chemical oxidation and electrochemical oxidations methods are most widely used to prepare PANI. The conducting form of PANI (emaraldine salt) is synthesized in acidic conditions due to doping of aniline monomers [32]. Besides PANI, its composites with inorganic materials like Cd, Ag, ZnO, TiO_2, SiO_2, MnO_2, and Fe_3O_4 have also been applied as efficient adsorbents by many researchers [33–37].

Altun and Ecevit [38] synthesized composites of cherry kernel shell pyrolytic charcoal with chitosan and Fe_2O_3 nanoparticles to remove Cr(VI) from aqueous solution. The data obtained were fitted in the Langmuir isotherm model and maximum adsorption of Cr(VI) was, respectively, 14.455 $mg.g^{-1}$ and 47.576 $mg{\cdot}g^{-1}$ for cherry kernel shell pyrolytic charcoal (CKSPC) and its composites with Fe_2O_3 (Fe-CCKSPC). Maleki et al. [39] synthesized amorphous aluminosilicate and its composites with Fe_3O_4 nanoparticles. These materials were applied as efficient adsorbents for removal of Cu(II), Cd(II), Hg(II), Pb(II), and Ni(II) from industrial effluents. The effects of initial concentration, pH, contact time, and temperature on adsorption phenomenon were investigated. The percent removal efficiency of the adsorption for Hg, Cd, Pb, Ni, and Cu were found to be 92%, 96%, 99%, 92%, and 99%, respectively. Cui and co-workers [40] synthesized polyaniline/attapulgite (PANI/ATP) composites by the chemical oxidation method to remove Hg (II) from aqueous environments. The maximum amount of Hg(II) adsorbed was 800 $mg{\cdot}g^{-1}$ at 5.9 solution pH and pseudo-second-order.

In the present study, PANI/Fe_3O_4 composites were synthesized through the chemical oxidation method. The synthesized composites were subsequently utilized to remove Cr(VI) and Ni(II) from aqueous environments. The adsorption behaviors of the composites were compared with pristine PANI and Fe_3O_4. Various techniques such as SEM, EDX, UV, and FTIR were used to characterize all the synthesized materials. Adsorption parameters such as the effect of time, pH, initial concentrations, temperature, adsorbent dosage, and ionic strength were also investigated. An atomic absorption spectrophotometer was used to find the amount of Cr(VI) and Ni(II) before and after adsorption.

Adsorption data were fitted in the Freundlich, Langmuir, Dubinin–Radishkevitch (D-R), Tempkin, and Elovich isotherm models. Kinetics of adsorption and thermodynamic parameters were determined.

2. Experimental

2.1. Materials

Aniline (Across) was distilled twice before use through vacuum distillation. Dodecyl benzene sulphonic acid (DBSA, Across), ferrous sulfate heptahydrate (Merck), ferric chloride hexahydrate (Sigma–Aldrich), hydrochloric acid (Merck), sodium sulfate (Panreac Quimica SA), potassium dichromate, and nickel (II) sulfate heptahydrate (Analar) were used. All chemicals used were analytically grade.

2.2. Batch Adsorption Study

PANI, Fe_3O_4 and their composites were synthesized as per our previous reports [41,42].

Solutions of both Cr(VI) and Ni(II) in different concentrations in the range of 5–100 mg·L^{-1} were prepared in 20 mL volumes from stock solution. A known amount of PANI/Fe_3O_4 composite was added to these solutions and shaken for about 90 min in a water bath shaker. These solutions were then filtered and the amount of Cr(VI) and Ni(II) ions in the filtrate were determined using an atomic absorption spectrophotometer by applying Equation (1) [40].

$$q_e = \frac{(C_0 - C_t)}{m} V \quad (1)$$

where C_0 (mg·L^{-1}) represents initial concentration and C_e (mg·L^{-1}) is the equilibrium concentration of heavy metals. Similarly, q_e (mg·g^{-1}) is the heavy metals adsorbed at equilibrium. m (g) refers to the mass of the adsorbent and V is the volume of the solution in mL. The effects of different parameters such as temperature, initial concentration, contact time, ionic strength, and pH on adsorption were studied. The data obtained from adsorption were also used to calculate the kinetics and thermodynamic properties. The same procedure was also used to study removal of Cr(VI) and Ni(II) through Fe_3O_4 and PANI. Desorption of Cr(VI) and Ni(II) were carried out by washing the adsorbents with double distilled water several time in a filter paper. Then 0.01 M sodium hydroxide was used to remove the remaining Cr(VI) while 0.01 M HCl was applied to remove Ni(II) ions.

2.3. Characterization

Surface morphologies of all adsorbents before and after adsorption were investigated with a scanning electron microscope (JSM-6490-JEOL, Tokyo, Japan). A Fourier transmission infrared spectrophotometer (Shimadzu, Tokyo, Japan) was used to record FTIR spectra of the PANI, and Fe_3O_4 and Fe_3O_4/PANI composites in the spectral range of 400– 4000 cm^{-1}. Elemental compositions of all adsorbents were determined through energy-dispersive X-ray (EDX) spectrophotometry (Oxford, UK, Inca 200). The amount of heavy metals adsorbed on the adsorbent materials was also determined with UV-Visible spectrophotometer (PerkinElmer, Buckinghamshire, UK). The amount of Cr(VI) and Ni(II) in water before and after adsorption was determined through atomic absorption spectrophotometry (A.Analyst 700, Perkin Elmer, Waltham, MA, USA).

3. Results and Discussion

3.1. Characterization

Morphological and structural features of all the adsorbents materials before and after adsorption were determined through various characterization techniques as discussed below.

3.1.1. SEM Study

Surface morphology and average size diameter of synthesized materials were investigated through SEM. Figure 1a–c shows SEM images of Fe_3O_4, PANI, and PANI/Fe_3O_4 respectively before adsorption. Iron oxides have a spherical morphology and an average particles size of 0.07 µm (70 nm) and are highly porous. It can be observed that these particles are agglomerated to each other which may be due to van der Waals forces. Existence of such forces has been observed in the earlier work [43]. PANI shows cabbage leaf like morphology, in which the polymers chains are adhered to each other through hydrogen bonding. After formation of composites with Fe_3O_4 particles, the morphology of PANI becomes sponge like and highly porous. Although visibility of Fe_3O_4 particles in the composites is not clear due to PANI layer formation, on close observation some bright and dark images of the core-shell like microsphere composites structures can be seen in the composite texture [44]. After adsorption of Cr(VI), the surface morphology of Fe_3O_4 slightly changes from spherical to rough due to interactions of Cr(VI) with active sites on the surface of Fe_3O_4. Figure 1d shows that the average diameter of the Fe_3O_4 particles increased to 0.18 µm (180 nm) as reported elsewhere [45]. The visibility of sphericalness became clearer when Ni(II) adhered onto Fe_3O_4. The average diameter of Fe_3O_4 particles increased to 0.09 µm (90 nm) after adsorption of Ni(II). Figure 1e,h shows SEM images of PANI after removal of Cr(VI) and Ni(II) respectively. As mentioned above, PANI showed cabbage leaf like morphology before adsorption which changed into cauliflower like shape when Cr(VI) and Ni(II) ions came in contact with the surface of PANI. Similarly cloudiness in the morphology of composites after adsorption of Cr(VI) and a cluster of ball like Ni(II) particles appeared after their adsorption as shown in Figure 1f,i. Similar results were observed in an earlier work where polypyrrole was used as an adsorbent to remove nickel from aqueous solution [46].

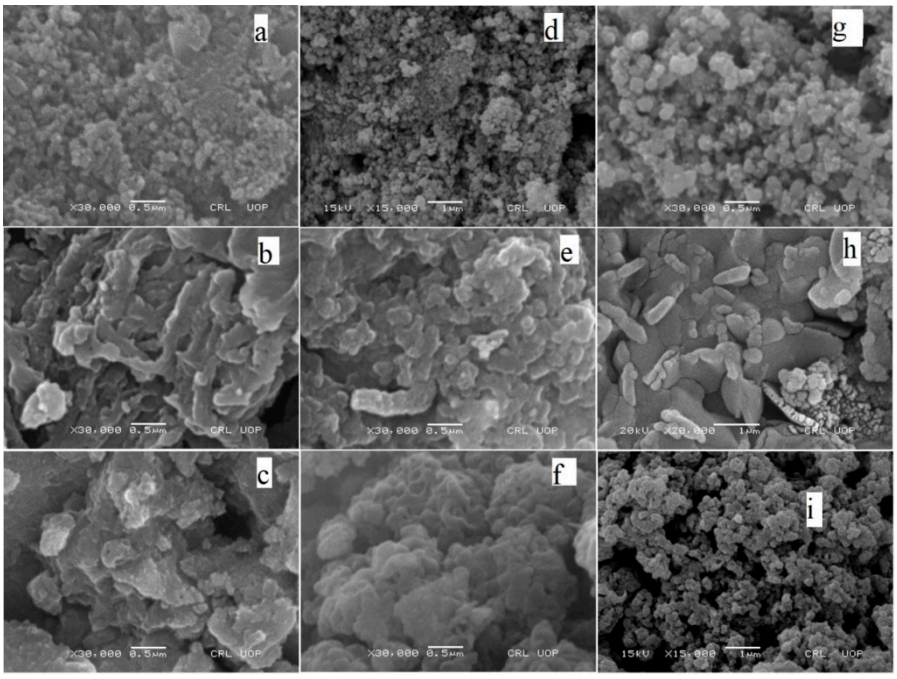

Figure 1. SEM images of Fe_3O_4, PANI (polyaniline). and PANI/Fe_3O_4 composites (**a**–**c**) before adsorption, (**d**–**f**) after Cr(VI) adsorption, and (**g**–**i**) after Ni(II) adsorption.

3.1.2. EDX Study

EDX spectra of iron oxide, PANI, and PANI/Fe_3O_4 composites before adsorption are shown in Figure 2a–c. These spectra show that percentages of Fe and O by weight were 65.05% and 34.95%, respectively, in Fe_3O_4. PANI was composed of 66.17% carbon and 16.97% nitrogen by weight. Besides carbon and nitrogen some other elements like oxygen, sulfur, iron and chlorine were also present in

the PANI texture. Existence of oxygen and sulfur indicate the presence of some moiety of DBSA in PANI, while iron and chlorine may be due to ferric chloride which was used as an oxidant. In the case of composites, percent weight of iron and oxygen were increased to 9.59% and 17.92%, respectively, while those of carbon and nitrogen were decreased to 61.45% and 6.60%. Figure 2d–f represent spectra recorded after adsorption of Cr(VI) on Fe_3O_4, PANI, and PANI/Fe_3O_4. Appearance of Cr and Ni indicates adherence of these elements to the adsorbent materials (Figure 2g–i). On close observation one can find a higher weight percentage of Cr(VI) than Ni(II).

Figure 2. Energy Dispersive X-ray (EDX) spectra of Fe_3O_4, PANI, and PANI/ Fe_3O_4 before adsorption (**a**–**c**), adsorption of Cr (VI) (**d**–**f**) and Ni (II) (**g**–**i**).

3.1.3. UV-Visible Study

Electronic and optical properties of materials can be determined by UV-Vis spectroscopy. Figure 3a,d,g shows the UV-Visible spectra of Fe_3O_4, PANI, and PANI/Fe_3O_4 before adsorption in N-methyl pyrrolidone (NMP). In the spectrum of iron oxide, a peak at 386.89 nm is due to the interaction of incident radiation with the outer most shell electrons of Fe in iron oxide. As a result, these electrons start to oscillate with the frequency of incident radiations showing surface plasmon resonance phenomenon (SPR) [46]. Another peak at 535.42 nm shows the presence of the DBSA moiety which was used as an emulsifying agent as reported elsewhere [47].

The spectrum of PANI showed a peak at 316.11 nm which corresponds to the $\pi-\pi^*$ transition of benzoinoid while another peak at 611.29 nm can be attributed to quinoid ring excitation as shown

in Figure 3d. Both these peaks are the characteristics absorption bands of the emaraldine base [48]. Deprotonation of emaraldine salt may occur due to formation of hydrogen bonds between hydrogens attached to amine group of PANI and the C=O group of NMP [49].

Formation of PANI/Fe_3O_4 composites can be characterized with two characteristics bands observed at 329.15 and 643.42 nm adsorption as shown in Figure 3g. Band at 643.42 nm can be assigned to the transfer of charge from the benzenoid to quinoid ring while the other band observed at 329.15 nm is attributed to the excitation of π electrons in the benzenoid ring. In the early research work, red shift is observed in the bipolaron band due to the doping of the amine group of benzenoid with Fe_3O_4 [50].

Removal of Cr(VI) through Fe_3O_4, PANI, and PANI/Fe_3O_4 composites was conducted by the UV-visible spectrum as shown in Figure 3b,e,h, while Figure 3c,f,i shows the same for Ni(II). The typical bands of the adsorbent materials were shifted to longer wavelengths, suggesting some physical interactions of these metals with active sites present on the surfaces of adsorbent materials. Cr(VI) cause more red shift as compared to Ni(II). Enhancement in Cr(VI) adsorption can be attributed to its larger size which can exist as $HCrO_4^-$ in aqueous solution, thus causing greater London or dispersion forces [51]. The intensity of the peak at 378.11 nm increased when Cr(VI) came in contact with the surface of composite materials as shown in Figure 3h. In our already published work, it was explained that doping of PANI with Fe_3O_4 caused an increase in the surface area of the composite resulting in the enhancement of adsorption [42].

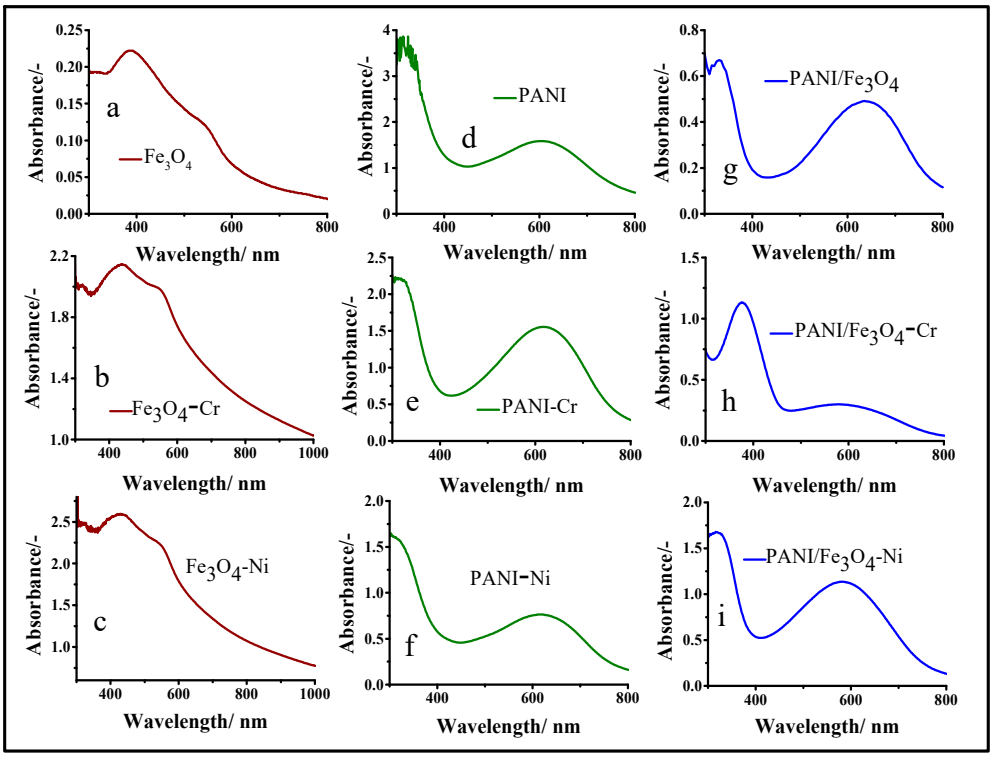

Figure 3. UV-visible spectra of Fe_3O_4, PANI, and PANI/Fe_3O_4 (**a**–**c**) before adsorption, (**d**–**f**) after adsorption of Cr(VI), and (**g**–**i**) after adsorption of Ni(II).

3.1.4. FTIR Study

A FTIR study was conducted to detect the characteristic groups of PANI and its composites with Fe_3O_4 before and after removal of Cr(VI) and Ni(II) as shown in Figure 4a–i. Significant peaks observed at 536.6 and 855.9 cm^{-1} corresponded to the Fe–O bond stretching vibrations in the spectrum of Fe_3O_4, thus confirming its formation. Similarly, a peak at 3466.4 cm^{-1} was attributed to the stretching vibrations due to the –OH group attached to the surface of Fe_3O_4. The presence of DBSA in the vicinity of Fe_3O_4 was also confirmed by the peak at 1649.6 cm^{-1} which showed the stretching vibration of the

$-CH_2-$ group present in the texture of DBSA. Khalaf et al. have observed Fe−O bond stretching at 550 cm^{-1} in SiO_2 coated Fe_3O_4 particles [52].

A FTIR spectrum of pristine PANI before adsorption is shown in Figure 4d. A characteristic peak showing the C−N−C bending mode in the aromatic ring appears at 574.7 cm^{-1}. Another peak at 667.9 cm^{-1} can be assigned to bending mode vibrations due to the C−C bond in the aromatic ring. Peaks at 819.6 and 1121.3 cm^{-1} were attributed to the bending vibrations due to out plane and in plane C−H bonds in the benzenoid ring [53]. Similarly, a peak appearing at 1309.5 cm^{-1} shows stretching vibrations due to $-C-N^+$ in the secondary aromatic amine. Thao et al. have synthesized polypyrrole/polyaniline composite through the interfacial polymerization method and observed stretching vibrations due to $-C-N^+$ of the secondary aromatic amine in the pristine PANI at 1297 cm^{-1} [54]. Peaks at 1461.4 and 1592.9 cm^{-1} can be assigned to C=N and C=C stretching vibrations of the quinoid and benzenoid rings of the PANI texture. The presence of DBSA moiety in the PANI backbone was also confirmed by the peak appearing at 1005.8 cm^{-1}, which was attributed to the stretching vibration due to S=O bond of $-SO_3H$ group [55]. Symmetric and asymmetric stretching vibrations due to the C–H bonds in PANI were represented respectively by two peaks at 2840.3 and 2933.3 cm^{-1}. Formation of PANI/Fe_3O_4 composites were confirmed by a weak peak at 511.2 cm^{-1} which corresponded to the stretching vibration due to the Fe−O bond in Fe_3O_4 as shown in Figure 4g. Moreover, the intensity of peaks at 2813.1 and 2926.5 cm^{-1} decreased, showing some interactions between the active sites present on the PANI surface and Fe_3O_4 particles. Interactions between PANI and Fe_3O_4 particles in composite materials were also observed in the slight shift in % transmittance towards longer wavelength regions as reported elsewhere [56].

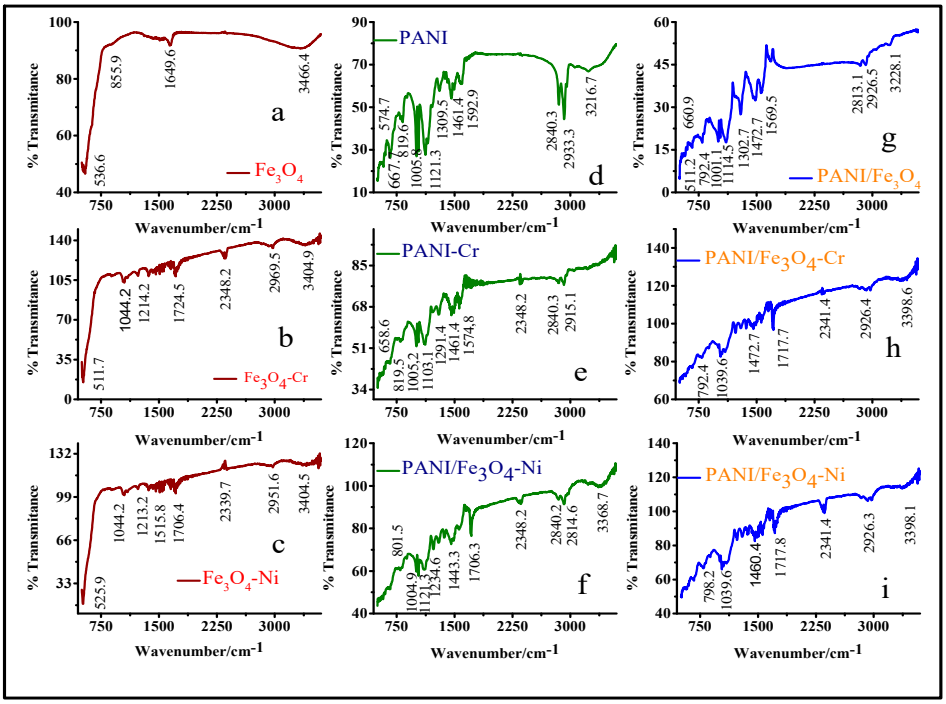

Figure 4. FTIR spectra of Fe_3O_4, PANI, and PANI/Fe_3O_4 composites (**a**,**d**,**g**) before adsorption, (**b**,**e**,**h**) after Cr(VI) adsorption, and (**c**,**f**,**i**) after Ni(II) adsorption.

After adsorption of Cr(VI), a slight shift towards low frequency range was observed in all peaks in the spectra of Fe_3O_4, PANI, and composite materials thus indicating some coating of chromium on adsorbents. Moreover, in the spectrum of Fe_3O_4 after adsorption of Cr(VI), peaks at 3404.9 and 2969.5 cm^{-1} were attributed to the stretching and bending vibrations due to the O−H bond of water molecules [43]. A peak present at 1724.5 cm^{-1} was associated to hydroxyl group deformation vibrations. Similarly a peak appeared at 1044.2 cm^{-1} which indicated intrinsic vibrations of the Cr−O bond, thus

confirming the adherence of Cr(VI) on to Fe_3O_4. Adsorption of Cr(VI) onto PANI was determined by the increase in intensity of the peak at 1005.2 cm^{-1} while in composites the same was observed at 1039.6 cm^{-1} as reported elsewhere [57,58]. Similar results were obtained after adsorption of Ni(II) on all adsorbent materials, however; shifting of % transmittance was less as compared to Cr(VI), indicating stronger interactions between Cr(VI) and adsorbent materials as compared to Ni(II) [59]. FTIR results correlated to the results obtained from EDX and UV-visible spectroscopy.

3.2. Adsorption Isotherm

An adsorption study mainly depends upon the interaction between adsorbents and pollutants. These interactions can be clearly understood by considering the adsorption isotherms. Various types of isotherms like Dubinin–Radushkevitch (D–R), Langmuir, Freundlich, and Tempkin isotherm models have been successfully applied by earlier researchers [60–62]. In the present study, the data were fitted into Langmuir, Freundlich, Tempkin, Dubinin–Radushkevitch (D–R), and Elovich isotherm models shown in Figure 5. Various adsorption parameters were calculated from these models shown in Table 1.

Table 1. Isotherm parameters calculated for Cr(VI) and Ni(II) adsorbed on Fe_3O_4, PANI, and Fe_3O_4/PANI composites.

Isotherms	Parameters	Adsorbents and Heavy Metals Adsorbed					
		Fe_3O_4		PANI		PANI/Fe_3O_4	
		Ni^{+2}	Cr^{+6}	Ni^{+2}	Cr^{+6}	Ni^{+2}	Cr^{+6}
Freundlich	1/n	0.2987	0.3688	0.3545	0.4716	0.2139	0.3905
	Kf	6.9559	35.026	39.244	26.119	55.523	53.801
	R^2	0.9366	0.9472	0.9232	0.9890	0.9307	0.9684
Langmuir	q_{max}	13.209	64.339	51.379	82.284	134.88	174.09
	k_L	20.554	25.877	111.59	66.374	900.52	1564.2
	R_L	0.0242	0.0198	0.0448	0.0753	0.0555	0.0324
	R^2	0.8136	0.9325	0.9068	0.9246	0.9184	0.8615
Tempkin	B	2.799	7.488	18.989	09.041	8.7281	24.414
	k_T	1.302	19.96	114.13	102.217	90.838	95.693
	R^2	0.811	0.912	0.952	0.897	0.798	0.902
D–R	q_s	39.056	37.412	45.695	43.243	62.053	62.427
	E_{ads}	22.499	26.982	33.298	32.653	34.742	37.981
	R^2	0.9025	0.8979	0.9316	0.7748	0.7995	0.8277
Elovich	q_e	73.874	13.879	14.592	13.766	12.048	26.285
	k_E	0.08683	44.688	51.886	31.199	782.8354	21.519
	R^2	0.5588	0.8235	0.8197	0.8749	0.7998	0.8767

The Freundlich isotherm is the most common adsorption model and describes the formation of multilayers by the molecules of pollutants on the surface of adsorbent materials. It also explains heterogeneity of adsorption due to different interactions between pollutants and adsorbents. A linearized form of Freundlich adsorption isotherm equation has been expressed by the following Equation (2).

$$\ln q_e = \ln K_f + \frac{1}{n} \ln C_e \quad (2)$$

where K_f is constant known as the Freundlich constant, 1/n is the slope referring to the adsorbent intensity, C_e ($mg \cdot L^{-1}$) is the remaining concentration of heavy metals at equilibrium, and q_e ($mg \cdot g^{-1}$) shows adsorption of heavy metals by one gram of adsorbent at equilibrium. Figure 5a shows the Freundlich isotherm graph obtained by plotting $\ln q_e$ vs. $\ln C_e$. From the intercept and slope of this graph the constants K_F and 1/n were calculated, which relate respectively to the adsorption capacity

and the adsorption intensity. Table 1 shows that 1/n values for adsorption of Ni(II) were 0.2987, 0.3545, and 0.2139 while for adsorption of Cr(VI) these values were 0.3688, 0.4716, and 0.3905 respectively, on Fe_3O_4, PANI, and PANI/Fe_3O_4 composites. These results showed high favorability of adsorption over the entire range of concentrations and closely resembled already published research works [58]. Moreover, by comparing the values of 1/n after adsorption of Cr(VI) and Ni(II) ions over all three adsorbents (Fe_3O_4, PANI, and PANI/ Fe_3O_4 composites), one can deduce that Cr(VI) shows more heterogeneity as compared to Ni(II). Ren et al. has reported that when the value of 1/n is smaller than one but more than zero ($1 > 1/n > 0$) the adsorption is highly favorable and heterogeneous, but when its values are more than unity ($1 < 1/n$) adsorption is unfavorable. However, if $1/n = 0$, adsorption is irreversible. Similarly, when the value of 1/n is unity then system is at equilibrium and homogeneous [43].

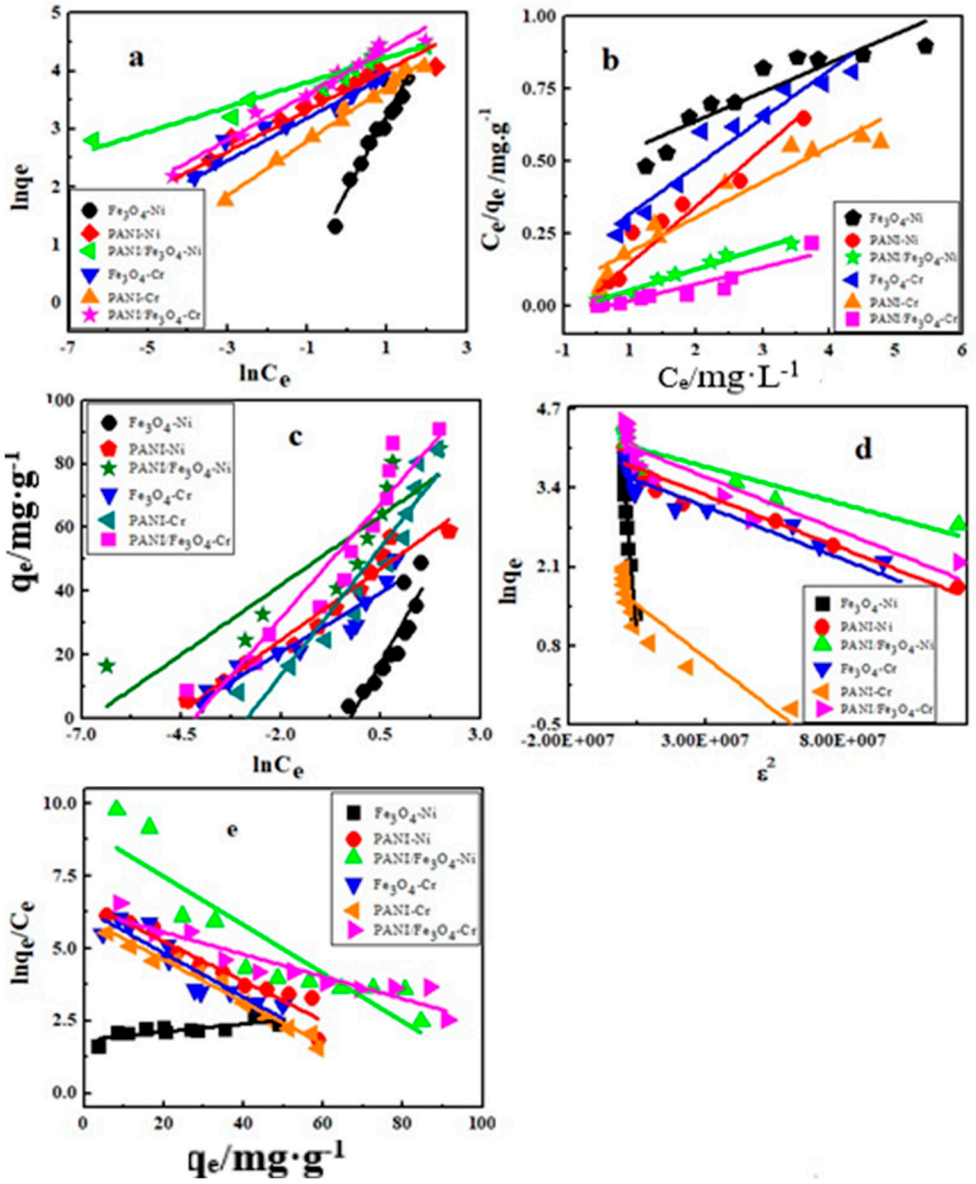

Figure 5. Adsorption isotherms (**a**) Freundlich, (**b**) Langmuir, (**c**) Tempkin, (**d**) Dubinin–Radushkevich (D–R), and (**e**) Elovich models of Cr(VI) and Ni(II) adsorbed on Fe_3O_4, PANI, and PANI/ Fe_3O_4 composites.

The Langmuir adsorption isotherm is another important model which expresses that adsorption of heavy metals occurs homogeneously resulting in the formation of a monolayer without interaction between the absorbed materials. It is expressed by the following Equation (3):

$$\frac{C_e}{q_e} = \frac{1}{q_{max}K_L} + \frac{1}{q_{max}C_e} \quad (3)$$

where K_L is constant called the Langmuir constant, q_{max} ($mg{\cdot}g^{-1}$) refers to maximum adsorption, q_e ($mg{\cdot}g^{-1}$) is the amount of heavy metals adsorbed at equilibrium, and C_e ($mg{\cdot}L^{-1}$) is the remaining concentration of heavy metals when equilibrium is established. Figure 5b shows a Langmuir isotherm plot between C_e/q_e and C_e. The adsorption maximum of Cr(VI) as well as Ni(II) on Fe_3O_4, PANI, and PANI/Fe_3O_4 composites were obtained from the slope of Figure 5b. These values are 13.209, 51.379, and 134.88 $mg{\cdot}g^{-1}$ for adsorption of Ni(II) onto Fe_3O_4, PANI, and PANI/Fe_3O_4 composites, while for Cr(VI) these value were respectively 64.339, 82.284, and 174.09 $mg{\cdot}g^{-1}$ onto Fe_3O_4, PANI, and PANI/Fe_3O_4 composites (Table 1). The results show enhancement in the adsorption of Cr(VI) as well as Ni(II) on composite materials as compared to pristine PANI and Fe_3O_4. Moreover, high values of q_{max} for Cr(VI) indicated strong interactions of Cr(VI) with adsorbent materials as compared to Ni(II). High adsorption of Cr(VI) was attributed to its existence as oxyanions (CrO_4^{2-}, $Cr_2O_7^{2-}$, and $HCrO_4^{-}$) in aqueous environments which may cause greater interactions with positively charged sites present on the surface of adsorbents. Similar results were shown in the already published work [63].

A dimensionless constant, also called separation factors (R_L), can be calculated by using the initial concentrations of pollutants (C_0) and constant K_L according to Equation (4) shown below:

$$R_L = \frac{1}{(1 + K_L C_0)} \quad (4)$$

Table 1 shows R_L values for Cr(VI) and Ni(II) adsorbed on Fe_3O_4, PANI, and PANI/Fe_3O_4 composites. The results closely resembled previously published reports which demonstrated that adsorption was favorable if the R_L value was more than zero but less than unity ($1 > R_L > 0$), unfavorable ($1 < R_L$), irreversible ($R_L = 0$), and linear ($R_L = 1$) [64].

Adsorption data were also fitted in the Tempkin isotherm to express the binding interactions of Cr(VI) and Ni(II) with adsorbent material shown by Figure 5c. It is expressed by the following Equation (5):

$$q_e = \beta \ln K_T + \beta \ln C_e \quad (5)$$

From the intercept of this equation, the binding constant (K_T) was calculated, which corresponds to the maximum binding energy of Cr(VI) and Ni(II) with adsorbent materials. Its values shown in the Table 1 suggest existence of strong binding forces between pollutants and adsorbents, thus correlated to the results of UV-visible, EDX, and FTIR analysis. By comparing these values, one can conclude that compared to Ni(II), oxyanions (CrO_4^{-2}, $Cr_2O_7^{-2}$, and $HCrO_4^{-}$) of Cr(VI) constitute strong binding forces with Fe_3O_4, PANI, and Fe_3O_4/PANI composites. β is another constant which can be obtained from the slope of the Tempkin isotherm. From the values of β, Tempkin isotherm constant (b) can be calculated according to Equation (6) as shown below:

$$\beta = \frac{RT}{b} \quad (6)$$

Tempkin isotherm constant b ($J{\cdot}mol^{-1}K^{-1}$) expresses heat of adsorption. The negative sign with the values of β showed that adsorption of Cr(VI) and Ni(II) on Fe_3O_4, PANI, and PANI/Fe_3O_4 composites is exothermic (Table 1) [65,66].

The Dubinin–Radushkevich (D–R) isotherm model is also very important and has been successfully applied by the earlier researchers. Its unique feature is differentiation between physical and chemical

adsorption and estimation of the energy of adsorption. The linear form of the D–R adsorption isotherm is described by the following Equation (7):

$$\ln q_e = \ln q_s - B\varepsilon^2 \quad (7)$$

where q_s ($mg \cdot g^{-1}$) represents the saturation capacity of adsorption. Figure 5d shows the D–R isotherm graph, obtained by plotting $\ln q_e$ vs. ε^2, where ε is polyanyi potential, which can be calculated according to Equation (8):

$$\varepsilon = RT\log(1+\frac{1}{C_e}) \quad (8)$$

where R ($J \cdot mol^{-1}K^{-1}$) is the general gas constant, C_e ($mg \cdot L^{-1}$) refers to the equilibrium concentration, and T is the Kelvin scale temperature. Energy of adsorption can be calculated by Equation (9) as expressed below:

$$E_{ads} = \frac{1}{\sqrt{(1-2B)}} \quad (9)$$

Using Equations (7) and (9), values of q_s and E_{ads} for Cr(VI) and Ni(II) adsorbed on Fe_3O_4, PANI, and PANI/Fe_3O_4 composite were calculated which indicated physical adsorption (Table 1). Similar results were shown by the already reported work which suggested that if the values of E_{ads} are less than 40 $kJ \cdot mol^{-1}$, the adsorption is physical, but values higher than 40 $kJ \cdot mol^{-1}$ suggest chemical adsorption [67]. Moreover, the typical range of ion-exchange process is 8–16 $kJ \cdot mol^{-1}$ [60]. In the present study, the E_{ads} value for adsorption of both Cr(VI) and Ni(II) were not in this range, which indicate that the ion-exchange process was not involved.

The Elovich isotherm linear form is represented as follow:

$$\ln \frac{q_e}{C_e} = \ln(k_E q_{max}) - \frac{1}{q_{max}} q_e \quad (10)$$

where q_{max} is the maximum capacity of adsorption, K_E ($L \cdot mg^{-1}$) refers to the Elovich constant and q_e is the amount of heavy metals adsorbed at equilibrium. From the slope and intercept of Figure 5e, values of q_{max} and K_E can be calculate (Table 1) [68]. R^2 values show that the Freundlich isotherm fit more closely than all other isotherms to the adsorption data.

3.3. Effect of pH on Adsorption

The pH of a solution greatly influences the behavior of adsorbents towards pollutants due to different interactions with them. The effect of pH on the removal of Cr(VI) and Ni(II) through Fe_3O_4, PANI, and PANI/Fe_3O_4 composites was determined by adjusting the pH of solutions in the range of 2–12 by adding some amount of 0.1 M HCl and 0.1 M NaOH as shown in Figure 6a. Concentration of each solution containing heavy metals was kept 50 $mg \cdot L^{-1}$. The graph shows that Cr(VI) adsorbed strongly in acidic media at pH less than 5 because at this pH chromium exists as an oxyanion (CrO_4^{-2}, $Cr_2O_7^{-2}$, or $HCrO_4^-$) in aqueous solution. Moreover, at lower pH negatively charged sites like the oxygen of iron oxide and the nitrogen of amine groups in the chains of PANI and composites are protonated. These positively charged sites of adsorbent cause electrostatic interactions with negatively charged CrO_4^{2-}, $Cr_2O_7^{2-}$, or $HCrO_4^-$ ions, thus adsorption becomes enhanced [69]. However, in basic medium, deprotonation of these sites causes electrostatic repulsions between adsorbents and dichromate ions, hence causing adsorption to decrease in basic medium. Xu et al. have studied the effect of pH on the removal of Cr(VI) by polypyrrole/calcium rectorite composite and reported that adsorption became decreased as the pH of the Cr(VI) ions solution increases [70]. The effect of pH on the removal of Ni(II) ions having 50 $mg \cdot L^{-1}$ concentrations was also studied from pH 2 to 12 at 30 °C shown in Figure 6b. The graph shows that adsorption of Ni(II) was less in acidic medium, because at lower pH, hydrogen ions may start to compete with Ni(II) ions for the surface active sites of adsorbents.

But as the pH increases, the amine and imine groups in PANI as well as in composites become free due to un-doping, hence resulting in the enhancement of adsorption. The highest adsorption of Ni(II) occurred at pH 7.5, but as the pH further increased, adsorption once again decreased. Less adsorption of Ni(II) in strong acidic and strong basic environments may be due to the existence of nickel as $Ni(OH)^+$ and $Ni(OH)_3^-$ respectively which may cause electrostatic repulsions with adsorbent materials. Early studies show that nickel exists in aqueous solutions as $Ni(OH)_3^-$, $Ni(OH)^+$, $Ni(OH)_2^0$, and Ni^{2+} depending on the pH of solution; however, it exists predominantly in Ni^{2+} form at pH 6–8 [71]. Shafiee et al. have demonstrated that Ni(II) forms complex due to precipitation at pH higher than 8, thus causing pore blockage at the surface of the adsorbent materials [72].

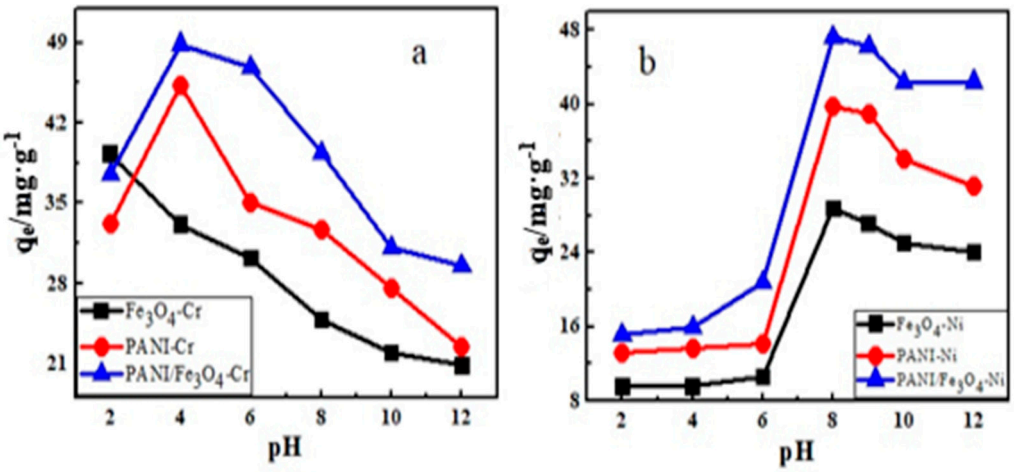

Figure 6. pH effect on removal of (**a**) Cr(VI), (**b**) Ni(II) through Fe_3O_4, PANI, and PANI/Fe_3O_4 composites.

3.4. Effect of Time and Temperature on Adsorption

Contact time between adsorbents and pollutants is very important for finding the equilibrium time during adsorption experiments. In the present work, the amount of Cr(VI) and Ni(II) adsorbed as a function of time on Fe_3O_4, PANI, and PANI/Fe_3O_4 composites were determined as shown in the Figure 7a. All the experiments were carried out by adding 0.035–0.036 g of each Fe_3O_4, PANI, and PANI/Fe_3O_4 composites to Cr(VI) and Ni(II) ion solutions. The pH of the Cr(VI) solution was adjusted at 3–4 while that of Ni(II) was adjusted to 7.5. The results show that initially the rate of adsorption was very high on all the adsorbent materials due to the presence of a large number of active sites. With the passage of time, these active sites were filled with Cr(VI) and Ni(II) ions which repelled further adsorption. As a result adsorption slowed down. By close observation of Figure 7a, it is clear that point of equilibrium was reached within 60–90 min for adsorbent materials [73]. Moreover, adsorption capacity of hybrid materials was higher than pure Fe_3O_4 and PANI. Figure 7b shows that adsorption was high at low temperatures and goes on to decrease as the temperature increased. This behavior showed the spontaneous and exothermic nature of adsorption and strongly correlated with the results shown by the Tempkin adsorption isotherm [74].

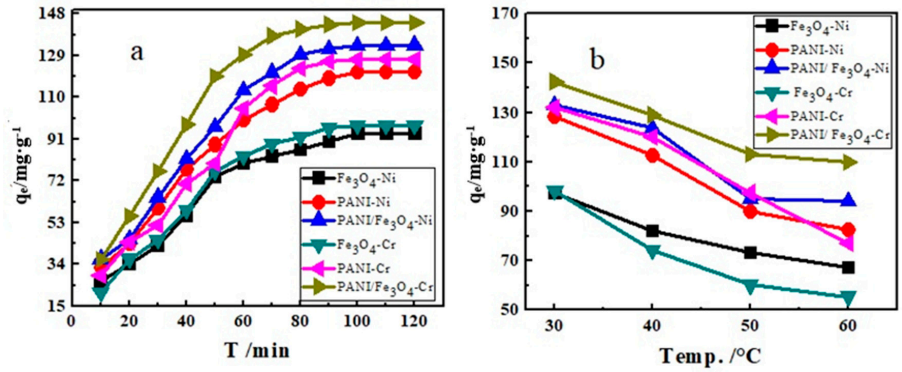

Figure 7. Effect of (**a**) contact time and (**b**) temperature on removal of Cr(VI) and Ni(II) ions through Fe_3O_4, PANI, and PANI/ Fe_3O_4 composites.

3.5. Effect of Adsorbent Dosage

The amount of adsorbent dosage in the solution of heavy metals also affects the adsorption process to great extant because of different surface areas. The effect of the adsorbent dose was determined by adding 0.034, 0.054, 075, 0.1, 0.13, and 0.16 g of Fe_3O_4, PANI, and PANI/Fe_3O_4 composites to 50 mg·L^{-1} solutions of Cr(VI) and Ni(II) ions separately. The pH of Cr(VI) was adjusted to 3–4 while that of Ni(II) was adjusted to 7.5 and the solutions were shaken for their corresponding equilibrium time. The results obtained are shown in Figure 8, which shows that removal efficiency of both Cr(VI) and Ni(II) ions depended upon the amount of adsorbent added. Enhancement in the removal of Cr(VI) and Ni(II) ions from the aqueous solution with adsorbent doses was attributed to the larger surface area and the large number of adsorption sites [75]. The results also show that removal efficiency of both Cr(VI) and Ni(II) was same up to 0.1 g of adsorbents but when the amount of adsorbent dose exceeded 0.1 g, the adsorption of Ni(II) became constant while that of Cr(VI) still increased and became constant after 0.14 g of adsorbent. This was due to hydration; Cr(VI) exists as CrO_4^{-2}, $Cr_2O_7^{-2}$, or $HCrO^{-4}$ in aqueous solution, which causes an increase in its size or volume. Due to this reason it needs a relatively large surface area and a large number of adsorbent sites as compared to nickel which exist as Ni^{+2} ions predominantly. As the concentrations of Cr(VI) and Ni(II) ions are constant, Ni(II) ions finish earlier than Cr(VI) in the aqueous solution [76].

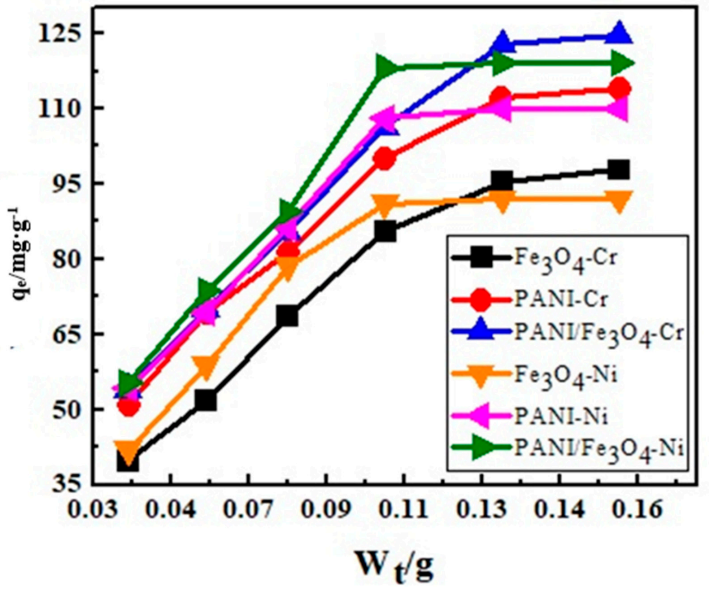

Figure 8. Effect of adsorbent dosage on adsorption of Cr(VI) and Ni(II).

3.6. Effect of Co-Existing Ions on Adsorption

The effluents coming out from industries contain several types of ions. These ions affect the surface properties of adsorbent materials. Sodium sulfate was chosen as an electrolyte to find the ionic strength effect on the removal of Cr(VI) and Ni(II) by Fe_3O_4, PANI, and PANI/Fe_3O_4 composites from aqueous environments. The concentration of both Cr(VI) and Ni(II) were kept constant (50 mg·L^{-1}) at a 20 mL volume. The pH ofthe Cr(VI) solution was adjusted to 2–4 while that of Ni(II) was adjusted to 7.5. Figure 9 shows the continuous decrease in the removal of both Cr(VI) and Ni(II) as the ionic strength increased from 0.01 to 0.1 then became constant [77]. In an acidic environment all active sites, like the oxygen of Fe_3O_4, the nitrogen present in amine, and the imine group of PANI and composites, become protonated. Under this condition chromium as well as sulfate ions also become hydrated as:

$$SO_4^{2-} + H^+ \longrightarrow HSO_4^-$$
$$Cr_2O_7^{2-} + H^+ \longrightarrow HCr_2O_7^-$$

These HSO_4^- and $HCr_2O_7^-$ compete with each other for positively charged active sites present on the surface of adsorbents. HSO_4^-, due to its smaller size, interacts faster with active sites of adsorbents as compared to $HCr_2O_7^-$, thus causing a decrease in the adsorption of $HCr_2O_7^-$. These results are supported by previously reported work which explained the effects of chloride and sulfate ions on the adsorption of chromium, nitrate, and phosphate ions [78]. Adsorption of Ni(II) was high at pH 7.5. At this pH, all the active sites present on the surface of all adsorbents become deprotonated and behave as negatively charged sites due to presence of a lone pair of electrons, hence sulfate ions have no effect on adsorption of Ni(II) ions. But under this condition, Na^+ ions start to compete with Ni(II) ions thus causing a decrease in its adsorption. Similar results have also been shown by already reported work [79]. From Figure 9, one can also deduce that initially the decrease in adsorption is fast, but as the ionic strength became 0.1, the decrease became relatively less and became nearly constant. This may be due to filling of all active sites by electrolyte ions as well pollutants.

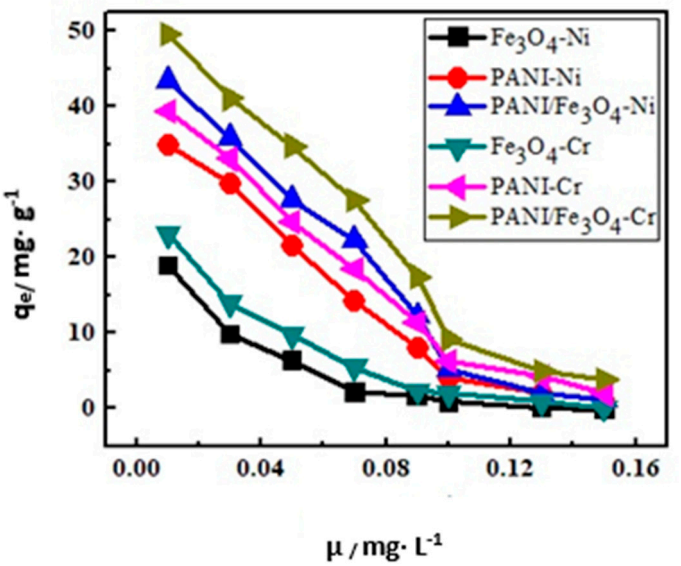

Figure 9. Effect of other ions on adsorption of Cr(VI) and Ni(II).

3.7. Kinetics of Adsorption

Knowledge of adsorption kinetics is a necessity to design kinetics models and to determine the adsorption mechanism. A number of kinetics models such as Lagergren's pseudo first order, Ho and McKay's pseudo second order, and Elovich and Weber and Morris's intra particle diffusion models have been tested by previous researchers [80].

In the present study, the adsorption data were also fitted in the pseudo first order and second order kinetics models. These models are expressed by the following Equations (11) and (12) respectively.

$$\log (q_e - q_t) = \log q_e - \frac{K_1 t}{2.303} \quad (11)$$

$$\frac{t}{q_t} = \frac{1}{K_2 q_e^{\,2}} + \frac{t}{q_e} \quad (12)$$

where q_t (mg·g^{-1}) and q_e (mg·g^{-1}) are the amount of heavy metals adsorbed after time "t" and equilibrium time respectively, K_1 and K_2 are the rate constants of pseudo first order (min^{-1}) and pseudo second order (g· mg^{-1} min^{-1}) respectively. "t" is the time in minutes and "C" is constant (mg· g^{-1}). Figure 10a shows a pseudo first order graph obtained by plotting ln(qe − qt) vs. t by using adsorption data of Cr(VI) and Ni(II) on Fe_3O_4, PANI, and composite materials respectively. From the slope of this graph, values of K1 from intercept qe values were determined as shown in Table 2. K1 is the time scaling factor and its values indicate how fast or slow the equilibrium is reached. In the present study, values of K1 for the adsorption of both Cr(VI) and Ni(VI) on Fe_3O_4, PANI, and PANI/Fe_3O_4 composites were of the following order (Fe_3O_4 > PANI > PANI/Fe_3O_4). It indicates that time of equilibrium was reached first by PANI/Fe_3O_4, then PANI, then Fe_3O_4. These results are in close agreement with already reported work [81]. Although all plots of Cr(VI) and Ni(II) adsorbed on all the three adsorbents have good linearity, the values of R^2 indicate that pseudo first order equations do not fit closely to the adsorption data. Therefore, a pseudo-second order kinetics model was tested for the adsorption data. Figure 10b shows the pseudo-second order plot obtained by plotting t/qt vs t. Values of the rate constant (K2) and equilibrium adsorption (q_e) were calculated from the intercept and slope respectively. The pseudo-second order model explained the behavior of adsorption over the whole range of time and closely agreed with the chemisorption mechanism. Values of R^2 indicated that the pseudo-second order kinetics model fit more closely to the adsorption data than the pseudo-first order model [82].

Table 2. Parameters of kinetics study of Cr(VI) and Ni(II) adsorption.

Adsorbents		Pseudo 1st Order			Pseudo 2nd Order		
		K_1 min^{-1}	q_e mg·g^{-1}	R^2	K_2 g·mg^{-1} min^{-1}	q_e mg·g^{-1}	R^2
Fe_3O_4	Ni^{2+}	0.226	22.23	0.926	0.0893	52.771	0.989
	Cr^{6+}	0.223	42.27	0.912	0.0551	62.973	0.994
PANI	Ni^{2+}	0.202	52.43	0.930	0.0133	80.580	0.997
	Cr^{6+}	0.127	64.38	0.645	0.0128	133.52	0.994
PANI/ Fe_3O_4	Ni^{2+}	0.201	82.14	0.865	0.0181	90.744	0.990
	Cr^{6+}	0.116	83.24	0.877	0.0078	145.98	0.980

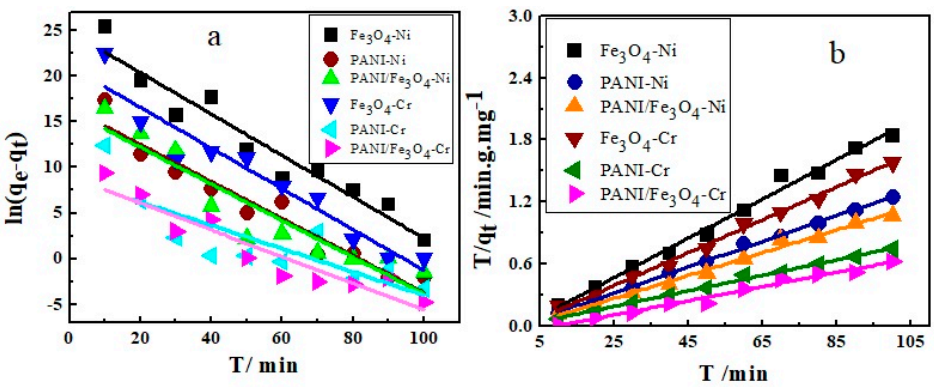

Figure 10. Kinetics of Cr(VI) and Ni(II) adsorption on Fe3O4, PANI, and PANI/Fe3O4 composites (**a**) first order and (**b**) second order kinetics model.

3.8. Thermodynamic of Adsorption

Adsorption behavior of Cr(VI) and Ni(II) ions on adsorbents can be investigated by studying the thermodynamic properties such as Gibb's Free energy, enthalpy, and entropy changes. In the present work, the change in the Gibb's Free energy (ΔG) was calculated with the help of Equation (13) as shown below:

$$\Delta G = -RT\ln\frac{q_e}{C_e} \tag{13}$$

Enthalpy (ΔH) and entropy changes (ΔS) were calculated from the slope and intercept of the Van't Hoff graph obtained by plotting $\ln q_e/c_e$ vs. 1/T as shown in Figure 11b. The Van't Hoff equation is expressed below:

$$\ln\frac{q_e}{C_e} = \frac{\Delta S}{R} - \frac{\Delta H}{RT} \tag{14}$$

where T is the absolute temperature and R ($J{\cdot}mol^{-1}k^{-1}$) is the general gas constant. The results obtained are summarized in Table 3. The negative sign with values of Gibb's free energy change and enthalpy and entropy change indicates the spontaneous and exothermic nature of adsorption. Moreover, the values of Gibb's Free energy change and enthalpy change show the existence of some electrostatic interactions between pollutants (Cr^{+6} and Ni^{+2}) and adsorbents thus showing physicochemical adsorption. This is in correlation with the previously reported work, which explain that for physical adsorption, the values of Gibb's free energy should range from −20 to zero $kJ{\cdot}mol^{-1}$, but when these values are more than this limit, the adsorption will be chemical [80]. Similarly Debnath et al. demonstrated that if the values of enthalpy change range from 84 to 420 $kJ{\cdot}mol^{-1}$, the adsorption will be chemical while when values of enthalpy change less than 84 $kJ{\cdot}mol^{-1}$ it indicates physical adsorption [83]. Besides these properties, activation energy also indicates the chemical and physical nature of adsorption. Its values have been calculated from the slope of Figure 11a obtained by plotting lnK vs. 1/T according to the Arrhenius equation as expressed below:

$$K = Ae^{-\frac{Ea}{RT}} \tag{15}$$

The values of activation energy shown in the Table 3 indicate physical adsorption. This result closely agrees with already reported works which indicate that if the values of activation energy range from 5 to 40 $kJ{\cdot}mol^{-1}$, the adsorption is physical. However, values of activation energy higher than 60 $kJ{\cdot}mol^{-1}$ indicate chemical adsorption. In the present work, the values activation energy for adsorption of Cr(VI) and Ni(II) on all the three adsorbents were less than 40 $kJ{\cdot}mol^{-1}$, thus adsorption was physical.

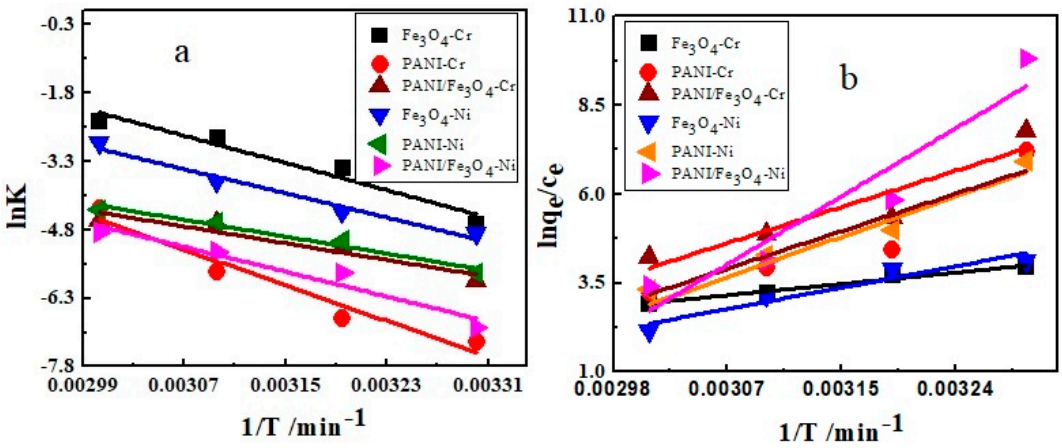

Figure 11. (**a**) Arrhenius plot and (**b**) Van't hoff plot of Cr(VI) and Ni(II) adsorption on Fe_3O_4, PANI, and PANI/ Fe_3O_4 composites.

Table 3. Thermodynamic properties of adsorption.

Parameters	Pollutants Adsorbed on Adsorbents					
	Fe_3O_4-Cr	PANI-Cr	PANI/ Fe_3O_4-Cr	Fe_3O_4-Ni	PANI-Ni	PANI/Fe_3O_4-Ni
ΔG (kJ·mol^{-1})	−05.61	−11.58	−19.91	v04.06	−09.75	−17.01
ΔH (kJ·mol^{-1})	−29.468	−44.205	−73.866	−25.432	−47.283	−76.46
Δ S (kJ·mol^{-1}K^{-1})	−14.043	−28.86	−24.25	−16.83	−26.712	−21.33
Ea (kJ·mol^{-1})	24.65	41.07	26.61	26.39	35.20	37.13

4. Conclusions

Fe_3O_4, PANI, and their composite can be applied as effective adsorbents for the removal of hexavalent chromium and divalent nickel from water. The adsorption of both Cr(VI) and Ni(II) was higher for composite material than Fe_3O_4 and PANI alone. This enhancement in adsorption might be due to the existence of electrostatic interactions between active sites on the surface of adsorbents with opposite charges of $HCrO_4^-$ and Ni (II$^{)}$ ions. Uptake of Cr(VI) on all the materials was high in an acidic environment while that of Ni(II) was high in a slightly basic environment. Adsorption of both metals decreased in the presence of co-existing ions. Removal of $HCrO_4^-$ was competed with by HSO_4^- in acidic environments while that of Ni(II) was competed with by Na^+ ions when the solution was slightly basic. The maximum decrease in the adsorption of both $HCrO_4^-$ and Ni(II) ions was observed at 0.1 ionic strength. The maximum amount of Cr(VI) adsorbed by PANI/Fe_3O_4 composites was 174.09 mg·g^{-1}, while that of Ni(II) was 134.88 mg·g^{-1}. The Freundlich adsorption isotherm model fitted more closely to the adsorption data. The kinetics of adsorption was pseudo-second order. The negative sign with the values of Gibb's free energy changes and enthalpy and entropy changes confirmed the spontaneous and exothermic nature of adsorption.

The presented tests were performed on a laboratory scale in very limited conditions of the external environment. As the effluents coming out from industries contain several types of ions, our future studies will focus on the implementation of this type of solution on an industrial scale in specific technical and climatic conditions.

Author Contributions: A.M. performed experimental work, formal analysis, and writing of the main draft. A.u.H.A.S. and S.B. supervised and contributed editing. All authors have read and agreed to the published version of the manuscript.

Funding: The APC was funded by the German Research Foundation and the Open Access Publication Funds of the Technische Universität Braunschweig.

Acknowledgments: We acknowledge support from the German Research Foundation and the Open Access Publication Funds of the Technische Universität Braunschweig. S.B. acknowledges support from the Alexander von Humboldt Foundation Germany.

Conflicts of Interest: The authors declare no conflict of interest.

References

1. Menon, M.C.; Patel, N.; He, J.C. Novel protein synthesis–breakdown complexes: TASCCed with fibrosis after G2-M arrest. *Kidney Int.* **2019**, *96*, 1056–1058. [CrossRef] [PubMed]
2. Gerek, E.E.; Yılmaz, S.; Koparal, A.S.; Gerek, Ö.N. Combined energy and removal efficiency of electrochemical wastewater treatment for leather industry. *J. Water Process Eng.* **2019**, *30*, 100382. [CrossRef]
3. Karlsson, M.C.; Álvarez-Asencio, R.; Bordes, R.; Larsson, A.; Taylor, P.; Steenari, B.M. Characterization of paint formulated using secondary TiO 2 pigments recovered from waste paint. *J. Coatings Technol. Res.* **2019**, *16*, 607–614. [CrossRef]
4. Tanihara, F.; Hirata, M.; Nguyen, N.T.; Le, Q.A.; Wittayarat, M.; Fahrudin, M.; Hirano, T.; Otoi, T. Generation of CD163-edited pig via electroporation of the CRISPR/Cas9 system into porcine in vitro-fertilized zygotes. *Anim. Biotechnol.* **2019**, *80*, 1–8. [CrossRef]
5. Zeng, Y.; Woo, H.; Lee, G.; Park, J. Adsorption of Cr (VI) on hexadecylpyridinium bromide (HDPB) modified natural zeolites. *Microporous Mesoporous Mater.* **2010**, *130*, 83–91. [CrossRef]

6. Costa, M. Potential hazards of hexavalent chromate in our drinking water. *Toxicol. Appl. Pharmacol.* **2003**, *188*, 1–5. [CrossRef]
7. Bayramoğlu, G.; Arica, M.Y. Adsorption of Cr (VI) onto PEI immobilized acrylate-based magnetic beads: isotherms, kinetics and thermodynamics study. *Chem. Eng. J.* **2008**, *139*, 20–28. [CrossRef]
8. Ding, J.; Pu, L.; Wang, Y.; Wu, B.; Yu, A.; Zhang, X.; Pan, B.; Zhang, Q.; Gao, G. Adsorption and reduction of Cr (VI) together with Cr (III) sequestration by polyaniline confined in pores of polystyrene beads. *Environ. Sci. Technol.* **2018**, *52*, 12602–12611. [CrossRef]
9. Yoshinaga, M.; Ninomiya, H.; Al Hossain, M.A.; Sudo, M.; Akhand, A.A.; Ahsan, N.; Alim, M.A.; Khalequzzaman, M.; Iida, M.; Yajima, I. A comprehensive study including monitoring, assessment of health effects and development of a remediation method for chromium pollution. *Chemosphere* **2018**, *201*, 667–675. [CrossRef]
10. Zhang, N.; Chen, M.; Li, J.; Deng, Y.; Li, S.-L.; Guo, Y.-X.; Li, N.; Lin, Y.; Yu, P.; Liu, Z. Metal nickel exposure increase the risk of congenital heart defects occurrence in offspring: A case-control study in China. *Medicine* **2019**, *98*, 15352. [CrossRef]
11. Saif, M.; Haq, M.; Memon, K. Heavy metals contamination through industrial effluent to irrigation water and soil in Korangi area of Karachi (Pakistan). *Int. J. Agric. Biochem.* **2005**, *4*, 646–648.
12. Sarwar, G.; Khan, J.; Iqbal, R.; Afridi, A.K.; Khan, A.; Sarwar, R. Bacteriological analysis of drinking water from urban and peri-urban areas of Peshawar. *J. Postgrad. Med. Inst.* **2011**, *18*, 64–69.
13. McGregor, D. lakes ecosystem linking traditional ecological knowledge and western science: aboriginal perspectives from the 2000 state of the lakes ecosystem te of the conference. *Can. J. Nat. Stud.* **2008**, *28*, 139–158.
14. Beluci, N.D.C.L.; Mateus, G.A.P.; Miyashiro, C.S.; Homem, N.C.; Gomes, R.G.; Fagundes-Klen, M.R.; Bergamasco, R.; Vieira, A.M.S. Hybrid treatment of coagulation/flocculation process followed by ultrafiltration in TIO2-modified membranes to improve the removal of reactive black 5 dye. *Sci. Environ.* **2019**, *664*, 222–229. [CrossRef]
15. Ghuge, S.P.; Saroha, A.K. Ozonation of Reactive Orange 4 dye aqueous solution using mesoporous Cu/SBA-15 catalytic material. *J. Water Process Eng.* **2018**, *23*, 217–229. [CrossRef]
16. Hao, J.; Ji, L.; Li, C.; Hu, C.; Wu, K. Rapid, efficient and economic removal of organic dyes and heavy metals from wastewater by zinc-induced in-situ reduction and precipitation of graphene oxide. *J. Tai. Inst. Chem. Eng.* **2018**, *88*, 137–145. [CrossRef]
17. Lafi, R.; Mabrouk, W.; Hafiane, A. Removal of Methylene blue from saline solutions by adsorption and electrodialysis. *Membrane Water Treat.* **2019**, *10*, 139–148.
18. Thaçi, B.S.; Gashi, S.T. Reverse Osmosis Removal of Heavy Metals from Wastewater Effluents Using Biowaste Materials Pretreatment. *Pol. J. Environ. Stud.* **2019**, *28*, 337–341. [CrossRef]
19. El-Said, A.; Badawy, N.; Garamon, S. Adsorption of heavy metal ions from aqueous solutions onto rice husk ash low cost adsorbent. *J. Environ. Anal. Toxicol.* **2018**, *8*, 1–5.
20. Noel, S.D.; Rajan, M. Impact of dyeing industry effluent on ground water quality by water quality index and correlation analysis. *Res. Biotechnol.* **2015**, *6*, 2657.
21. Kyzas, G.Z.; Bomis, G.; Kosheleva, R.I.; Efthimiadou, E.K.; Favvas, E.P.; Kostoglou, M.; Mitropoulos, A.C. Nanobubbles effect on heavy metal ions adsorption by activated carbon. *Chem. Eng. J.* **2019**, *356*, 91–97. [CrossRef]
22. Shi, J.; Fan, X.; Tsang, D.C.; Wang, F.; Shen, Z.; Hou, D.; Alessi, D.S. Removal of lead by rice husk biochars produced at different temperatures and implications for their environmental utilizations. *Chemosphere* **2019**, *235*, 825–831. [CrossRef] [PubMed]
23. Mohammad-Rezaei, R.; Jaymand, M. Graphene quantum dots coated on quartz sand as efficient and low-cost adsorbent for removal of Hg2+ and Pb2+ from aqueous solutions. *Environ. Prog. Sustain. Energy* **2019**, *38*, S24–S31. [CrossRef]
24. Zhu, J.; Chen, R.; Zeng, Z.; Su, C.; Zhou, K.; Mo, Y.; Guo, Y.; Zhou, F.; Gao, J.; Li, L. Acetone adsorption capacity of sulfur-doped microporous activated carbons prepared from polythiophene. *Environ. Sci. Pollut. Res.* **2019**, *26*, 16166–16180. [CrossRef] [PubMed]
25. Mahlangu, T.; Das, R.; Abia, L.K.; Onyango, M.; Ray, S.S.; Maity, A. Thiol-modified magnetic polypyrrole nanocomposite: An effective adsorbent for the adsorption of silver ions from aqueous solution and subsequent water disinfection by silver-laden nanocomposite. *Chem. Eng. J.* **2019**, *360*, 423–434. [CrossRef]

26. Ju, P.; Liu, Q.; Zhang, H.; Chen, R.; Liu, J.; Yu, J.; Liu, P.; Zhang, M.; Wang, J. Hyperbranched topological swollen-layer constructs of multi-active sites polyacrylonitrile (PAN) adsorbent for uranium (VI) extraction from seawater. *Chem. Eng. J.* **2019**, *374*, 1204–1213. [CrossRef]
27. Sowmiya, G.; Velraj, G.; Shanmugapriya, C. Investigation of enhanced ac electrical conductivity of nano aluminium particles doped with polymer composite by in-situ chemical oxidation polymerization method. *Adv. Nat. Appl. Sci.* **2017**, *11*, 168–173.
28. Deshmukh, V.; Paithankar, K.; Shelke, U.; More, S.; Iyyer, S.; Gade, V. Study of Influence for Various Parameters to Electro-chemical Synthesis of Polyaniline Thin Film by Galvanostatic Method. *Int. Res. J. Sci. Eng.* **2018**, 150–155.
29. Lei, Y.; Zhou, J.; Yao, Z.; Li, L. Self-assembly of porous polyaniline microspheres via template-free interfacial method for high-performance electromagnetic absorption property. *Mater. Lett.* **2020**, *265*, 127389. [CrossRef]
30. Freitas, T.V.; Sousa, E.A.; Fuzari, G.C., Jr.; Arlindo, E.P. Different morphologies of polyaniline nanostructures synthesized by interfacial polymerization. *Mater. Lett.* **2018**, *224*, 42–45. [CrossRef]
31. Chauhan, N.P.S.; Mozafari, M. *Synthetic route of PANI (II): Enzymatic method, in Fundamentals and Emerging Applications of Polyaniline*, 1st ed.; Elsevier: Amsterdam, The Netherlands, 2019; pp. 43–65.
32. Chauhan, K.; Mahajan, J. Synthesis and characterization of nano zinc oxide emeraldine salt composite. Int. *J. Sci. Res. Phy. Appl. Sci.* **2017**, *5*, 1–11.
33. Mota, M.L.; Carrillo, A.; Verdugo, A.J.; Olivas, A.; Guerrero, J.M.; De la Cruz, E.C.; Noriega, R.N. Synthesis and novel purification process of PANI and PANI/AgNPS composite. *Molecules* **2019**, *24*, 1621. [CrossRef] [PubMed]
34. Daikh, S.; Zeggai, F.; Bellil, A.; Benyoucef, A. Chemical polymerization, characterization and electrochemical studies of PANI/ZnO doped with hydrochloric acid and/or zinc chloride: differences between the synthesized nanocomposites. *J. Phys. Chem. Solids* **2018**, *121*, 78–84. [CrossRef]
35. Jia, Q.; Wang, W.; Zhao, J.; Xiao, J.; Lu, L.; Fan, H. Synthesis and characterization of TiO_2/polyaniline/graphene oxide bouquet-like composites for enhanced microwave absorption performance. *J. Alloys Compd.* **2017**, *710*, 717–724. [CrossRef]
36. Kai, W.; Liwei, L.; Wen, X.; Shengzhe, Z.; Yong, L.; Hongwei, Z.; Zongqiang, S. Electrodeposition synthesis of PANI/MnO_2/graphene composite materials and its electrochemical performance. *Int. J. Electrochem. Sci.* **2017**, *12*, 8306–8314. [CrossRef]
37. Wang, Y.; Wu, X.; Zhang, W.; Luo, C.; Li, J.; Wang, Q.; Wang, Q. Synthesis of polyaniline nanorods and Fe3O4 microspheres on graphene nanosheets and enhanced microwave absorption performances. *Mater. Chem. Phys.* **2018**, *209*, 23–30. [CrossRef]
38. Altun, T.; Ecevit, H. Cr (VI) removal using Fe2O3-chitosan-cherry kernel shell pyrolytic charcoal composite beads. *Environ. Eng. Res.* **2019**, *25*, 426–438. [CrossRef]
39. Maleki, A.; Hajizadeh, Z.; Sharifi, V.; Emdadi, Z. A green, porous and eco-friendly magnetic geopolymer adsorbent for heavy metals removal from aqueous solutions. *J. Clean. Prod.* **2019**, *215*, 1233–1245. [CrossRef]
40. Cui, H.; Qian, Y.; Li, Q.; Zhang, Q.; Zhai, J. Adsorption of aqueous Hg(II) by polyaniline/attapulgite composite. *Chem. Eng.* **2012**, *211*, 216–223. [CrossRef]
41. Muhammad, A.; Shah, A.H.A.; Bilal, S. Comparative Study of the Adsorption of Acid Blue 40 on Polyaniline, Magnetic Oxide and Their Composites: Synthesis, Characterization and Application. *Materials* **2019**, *12*, 2854. [CrossRef]
42. Muhammad, A.; Shah, A.H.A.; Bilal, S.; Rahman, G. Basic Blue Dye Adsorption from Water using Polyaniline/Magnetite (Fe_3O_4) Composites: Kinetic and Thermodynamic Aspects. *Materials* **2019**, *12*, 1764. [CrossRef] [PubMed]
43. Ren, G.; Wang, X.; Huang, P.; Zhong, B.; Zhang, Z.; Yang, L.; Yang, X. Chromium (VI) adsorption from wastewater using porous magnetite nanoparticles prepared from titanium residue by a novel solid-phase reduction method. *Sci. Tot. Environ.* **2017**, *607*, 900–910. [CrossRef] [PubMed]
44. Dastgerdi, Z.H.; Meshkat, S.S.; Hosseinzadeh, S.; Esrafili, M.D. Application of Novel Fe_3O_4–Polyaniline Nanocomposites in Asphaltene Adsorptive Removal: Equilibrium, Kinetic Study and DFT Calculations. *J. Inorg. Organomet. Polym. Mater.* **2019**, *29*, 1160–1170. [CrossRef]
45. Karamipour, A.; Parsi, P.K.; Zahedi, P.; Moosavian, S.M.A. Using Fe_3O_4-coated nanofibers based on cellulose acetate/chitosan for adsorption of Cr (VI), Ni (II) and phenol from aqueous solutions. *Int. J. Biol. Macromol.* **2019**, *25*, 435–446. [CrossRef]

46. Abdolmaleki, A.Y.; Eisazadeh, H.; Taghipour, Z.; Tanzifi, M. Effect of various agents on removal of Nickel from aqueous solution using polypyrrole as an adsorbent. *J. Eng. Sci. Technol.* **2012**, *7*, 540–551.
47. Tung, L.M.; Cong, N.X.; Huy, L.T.; Lan, N.T.; Phan, V.N.; Hoa, N.Q.; Vinh, L.K.; Thinh, N.V.; Tai, L.T.; Mølhave, K. Synthesis, characterizations of superparamagnetic Fe_3O_4–Ag hybrid nanoparticles and their application for highly effective bacteria inactivation. *J. Nanosci. Nanotechnol.* **2016**, *16*, 5902–5912. [CrossRef]
48. Gupta, A.; Kumar, M. The chemical synthesis and characterizations of silver-doped polyaniline: role of silver–solvent interactions. *Polym. Bullet.* **2020**, *77*, 1913–1928.
49. Zhao, X.-Y.; Xie, J.; Wang, M.-Z.; Xing, A. Synthesis and characterization of novel biodegradable tetra-amino-terminated PLGA telechelic copolymer. *J. Mater. Sci.* **2013**, *48*, 659–664. [CrossRef]
50. Hatamzadeh, M.; Johari-Ahar, M.; Jaymand, M. In situ chemical oxidative graft polymerization of aniline from Fe3O4 nanoparticles. *Int. J. Nanosci. Nanotechnol.* **2012**, *8*, 51–60.
51. Javadian, H.; Vahedian, P.; Toosi, M. Adsorption characteristics of Ni (II) from aqueous solution and industrial wastewater onto Polyaniline/HMS nanocomposite powder. *Appl. Surf. Sci.* **2013**, *284*, 13–22. [CrossRef]
52. Khalaf, M.M.; Al-Amer, K.; El-lateef, H.M.A. Magnetic Fe_3O_4 nanocubes coated by SiO2 and TiO2 layers as nanocomposites for Cr (VI) up taking from wastewater. *Ceram. Int.* **2019**, *45*, 23548–23560. [CrossRef]
53. Ahmad, R. Polyaniline/ZnO Nanocomposite: A Novel Adsorbent for the Removal of Cr (VI) from Aqueous Solution, in Advances in Composite Materials Development. *IntechOpen* **2019**, *1*, 1–22.
54. Thao, V.D.; Giang, B.L.; Thu, T.V. Free-standing polypyrrole/polyaniline composite film fabricated by interfacial polymerization at the vapor/liquid interface for enhanced hexavalent chromium adsorption. *RSC Adv.* **2019**, *9*, 5445–5452. [CrossRef]
55. Zamani, F.G.; Moulahoum, H.; Ak, M.; Odaci, D.; Timur, S. Current trends in the development of conducting polymers-based biosensors. 2012. *TrAC Trend. Anal. Chem.* **2019**, *118*, 264–276. [CrossRef]
56. Zanotto, C.; Ratuchne, F.; Guimarães de Castro, E.; Teixeira, M.P. Structural Characterization of Magnetite and its Influence on the Formation of Composites with Polyaniline. *Orbital: Electro. J. Chem.* **2019**, *11*, 427–432. [CrossRef]
57. Lyu, W.; Wu, J.; Zhang, W.; Liu, Y.; Yu, M.; Zhao, Y.; Feng, J.; Yan, W. Easy separated 3D hierarchical coral-like magnetic polyaniline adsorbent with enhanced performance in adsorption and reduction of Cr (VI) and immobilization of Cr (III). *Chem. Eng. J.* **2019**, *363*, 107–119. [CrossRef]
58. Seo, J.H.; Choi, C.S.; Bae, J.H.; Jeong, H.; Lee, S.-H.; Kim, Y.S. Preparation of a Lignin/Polyaniline Composite and Its Application in Cr (VI) Removal from Aqueous Solutions. *BioResource* **2019**, *14*, 9169–9182.
59. Amer, R.; Ossman, M.; Hassan, H.; Ghozlan, H.; Sabry, S. Adsorption of Ni (II) by Exiguobacterium sp. 27 and Polyaniline Nanoparticles. *Int. J. Environ. Res.* **2014**, *8*, 601–612.
60. He, Y.; Zhang, L.; An, X.; Wan, G.; Zhu, W.; Luo, Y. Enhanced fluoride removal from water by rare earth (La and Ce) modified alumina: Adsorption isotherms, kinetics, thermodynamics and mechanism. *Sci. Total Environ.* **2019**, *688*, 184–198. [CrossRef]
61. Guedidi, H.; Lakehal, I.; Reinert, L.; Lévêque, J.-M.; Bellakhal, N.; Duclaux, L. Removal of ionic liquids and ibuprofen by adsorption on a microporous activated carbon: kinetics, isotherms, and pore sites. *Arabian J. Chem.* **2020**, *13*, 258–270. [CrossRef]
62. Vergis, B.R.; Kottam, N.; Krishna, R.H.; Nagabhushana, B. "Removal of Evans Blue dye from aqueous solution using magnetic spinel ZnFe2O4 nanomaterial: Adsorption isotherms and kinetics. *Nano-Struct. Nano-Object.* **2019**, *18*, 100290. [CrossRef]
63. Dinari, M.; Soltani, R.; Mohammadnezhad, G. Kinetics and thermodynamic study on novel modified–mesoporous silica MCM-41/polymer matrix nanocomposites: effective adsorbents for trace CrVI removal. *J. Chem. Eng. Data* **2017**, *62*, 2316–2329. [CrossRef]
64. Goyal, S.; Goyal, V. Cr (VI) removal from synthetic textile effluent using Tamarindus indica bark: a kinetic and thermodynamic study. *Curr. Sci.* **2016**, *17*, 392–398.
65. Dehghani, M.H.; Sarmadi, M.; Alipour, M.R.; Sanaei, D.; Abdolmaleki, H.; Agarwal, S.; Gupta, V.K. Investigating the equilibrium and adsorption kinetics for the removal of Ni (II) ions from aqueous solutions using adsorbents prepared from the modified waste newspapers: A low-cost and available adsorbent. *Microchem. J.* **2019**, *146*, 1043–1053. [CrossRef]
66. Das, A.; Banerjee, M.; Bar, N.; Das, S.K. Adsorptive removal of Cr (VI) from aqueous solution: kinetic, isotherm, thermodynamics, toxicity, scale-up design, and GA modeling. *SN Appl. Sci.* **2019**, *1*, 776. [CrossRef]

67. Jorfi, S.; Shooshtarian, M.R.; Pourfadakari, S. Decontamination of cadmium from aqueous solutions using zeolite decorated by Fe_3O_4 nanoparticles: adsorption modeling and thermodynamic studies. *Int. J. Environ. Sci. Technol.* **2020**, *17*, 273–286. [CrossRef]
68. Nikzad, S.; Amooey, A.A.; Alinejad-Mir, A. Adsorption of diazinon from aqueous solutions by magnetic guar gum-montmorillonite. *Chem. Data Collect.* **2019**, *20*, 100187. [CrossRef]
69. Chigondo, M.; Paumo, H.K.; Bhaumik, M.; Pillay, K.; Maity, A. Magnetic arginine-functionalized polypyrrole with improved and selective chromium (VI) ions removal from water. *J. Mol. Liq.* **2019**, *275*, 778–791. [CrossRef]
70. Xu, Y.; Chen, J.; Chen, R.; Yu, P.; Guo, S.; Wang, X. Adsorption and reduction of chromium (VI) from aqueous solution using polypyrrole/calcium rectorite composite adsorbent. *Water Res.* **2019**, *160*, 148–157. [CrossRef]
71. Liu, D.; Deng, S.; Vakili, M.; Du, R.; Tao, L.; Sun, J.; Wang, B.; Huang, J.; Wang, Y.; Yu, G. Fast and high adsorption of Ni (II) on vermiculite-based nanoscale hydrated zirconium oxides. *Chem. Eng. J.* **2019**, *360*, 1150–1157. [CrossRef]
72. Shafiee, M.; Abedi, M.A.; Abbasizadeh, S.; Sheshdeh, R.K.; Mousavi, S.E.; Shohani, S. Effect of zeolite hydroxyl active site distribution on adsorption of Pb (II) and Ni (II) pollutants from water system by polymeric nanofibers. *Sep. Sci. Technol.* **2019**, 1–18. [CrossRef]
73. Jiang, D.; Yang, Y.; Huang, C.; Huang, M.; Chen, J.; Rao, T.; Ran, X. Removal of the heavy metal ion nickel (II) via an adsorption method using flower globular magnesium hydroxide. *J. Hazard. Mater.* **2019**, *373*, 131–140. [CrossRef] [PubMed]
74. Shen, Z.; Hou, D.; Jin, F.; Shi, J.; Fan, X.; Tsang, D.C.; Alessi, D.S. Effect of production temperature on lead removal mechanisms by rice straw biochars. *Sci. Total Environ.* **2019**, *655*, 751–758. [CrossRef] [PubMed]
75. Wu, H.; Wen, Q.; Hu, L.; Gong, M. Effect of adsorbate concentration to adsorbent dosage ratio on the sorption of heavy metals on soils. *J. Environ. Eng.* **2018**, *144*, 4017094. [CrossRef]
76. Padmavathy, K.; Madhu, G.; Haseena, P. A study on effects of pH, adsorbent dosage, time, initial concentration and adsorption isotherm study for the removal of hexavalent chromium (Cr (VI)) from wastewater by magnetite nanoparticles. *Proc. Technol.* **2016**, *24*, 585–594. [CrossRef]
77. Liang, Q.; Geng, J.; Luo, H.; Fang, W.; Yin, Y. Fast and selective removal of Cr (VI) from aqueous solutions by a novel magnetic Cr (VI) ion-imprinted polymer. *J. Mol. Liq.* **2017**, *248*, 767–774. [CrossRef]
78. Karthikeyan, P.; Elanchezhiyan, S.S.; Preethi, J.; Meenakshi, S.; Park, C.M. Mechanistic performance of polyaniline-substituted hexagonal boron nitride composite as a highly efficient adsorbent for the removal of phosphate, nitrate, and hexavalent chromium ions from an aqueous environment. *Appl. Surf. Sci.* **2020**, *511*, 145543. [CrossRef]
79. Ali, Z.T.A.; Naji, L.A.; Almuktar, S.A.; Faisal, A.A.; Abed, S.N.; Scholz, M.; Naushad, M.; Ahamad, T. Predominant mechanisms for the removal of nickel metal ion from aqueous solution using cement kiln dust. *J. Water Process Eng.* **2020**, *33*, 101033. [CrossRef]
80. Rahdar, S.; Rahdar, A.; Ahmadi, S.; Mehdizadeh, Z.; Taghavi, M. Preparation, Physical Characterization and Adsorption Properties of Synthesized Co–Ni–Cr Nanocomposites for Highly Effective Removal of Nitrate: Isotherms, Kinetics and Thermodynamic Studies. *Z Phys. Chem.* **2020**, *234*, 45–62. [CrossRef]
81. Wang, H.; Xu, C.; Yuan, B. Polymer-based Electrochemical Sensing Platform for Heavy Metal Ions Detection-A Critical Review. *Int. J. Electrochem. Sci.* **2019**, *14*, 8760–8771. [CrossRef]
82. Aamir, M. Investigating the Antibacterial Activity of POMA Nanocomposites. *Pol. J. Environ. Stud.* **2019**, *28*, 4191–4198.
83. Debnath, M.K.; Rahman, M.A.; Minami, H.; Rahman, M.M.; Alam, M.A.; Sharafat, M.K.; Hossain, M.K.; Ahmad, H. Single step modification of micrometer-sized polystyrene particles by electromagnetic polyaniline and sorption of chromium (VI) metal ions from water. *J. Appl. Poly. Sci.* **2019**, *136*, 47524. [CrossRef]